Non-mechanical sub-pixel image shifter for acquiring super-resolution digital images

Hsiao-Chin Lan,[1,2] Mount-Learn Wu,[2] and Eric M. Yeatman[1,*]

[1]*Department of Electrical and Electronic Engineering, Imperial College London, London, SW7 2AZ, UK*
[2]*Department of Optics and Photonics, National Central University, Jhong-li, 32001, Taiwan.*
**e.yeatman@imperial.ac.uk*

Abstract: A sub-pixel image shifter is presented, for use in enhancing the spatial resolution of digital image sensors by combining multiple displaced sub-images using a super-resolution (SR) algorithm. The device uses the walk-off phenomenon in birefringent crystals to separate images with opposite polarizations by a sub-pixel displacement. A liquid crystal (LC) waveplate plus a polarizer can then select the specific image to be exposed, with fast, non-mechanical control. This cascaded device, comprising two sapphire crystals, two LCs, and a single polarizer, is capable of 2-dimensional image shift with displacements of 0.5 pixels. The experimental results show that the image registration stability can be precisely controlled within 0.05 pixels and the contrast transfer function ratio of the SR image is enhanced by up to 1.36 times compared to the original captured image. Moreover, based on the fast transition time of LCs, the displaced sub-images can be recorded in video form with a frame rate of 40 fps.

OCIS codes: (100.6640) Super resolution; (100.0100) Image processing; (260.1440) Birefringence; (160.3710) Liquid crystals; (150.6044) Smart cameras.

References and links

1. W. Wolf, B. Ozer, and T. Lv, "Smart Cameras as Embedded Systems," IEEE Computer **35**(9), 48–53 (2002).
2. M. Bramberger, A. Doblander, A. Maier, B. Rinner, and H. Schwabach, "Distributed Embedded Smart Cameras for Surveillance Applications," IEEE Computer **39**(2), 68–75 (2006).
3. S. K. Nayar, "Computational Cameras: Redefining the Image," IEEE Computer **39**(8), 30–38 (2006).
4. M. Ben-Ezra, A. Zomet, and S. K. Nayar, "Video super-resolution using controlled subpixel detector shifts," IEEE Trans. Pattern Anal. Mach. Intell. **27**(6), 977–987 (2005).
5. C. Y. Gao, and N. Ahuja, "A refractive camera for acquiring stereo and super-resolution images," in *Proceedings of the 2006 IEEE Computer Society Conference on Computer Vision Pattern Recognition* (2006), pp. 2316–2323.
6. K. Yu, N. Park, D. Lee, and O. Solgaard, "Superresolution digital image enhancement by subpixel image translation with a scanning micromirror," IEEE J. Sel. Top. Quantum Electron. **13**(2), 304–311 (2007).
7. R. A. Hicks, V. T. Nasis, and T. P. Kurzweg, "Programmable imaging with two-axis micromirrors," Opt. Lett. **32**(9), 1066–1068 (2007).
8. A. Mohan, X. Huang, J. Tumblin, and R. Raskar, "Sensing increased image resolution using aperture masks," in *Proceedings of the 2008 IEEE Computer Society Conference on Computer Vision Pattern Recognition* (2008).
9. R. F. Marcia, C. Kim, C. Eldeniz, J. Kim, D. J. Brady, and R. M. Willett, "Superimposed video disambiguation for increased field of view," Opt. Express **16**(21), 16352–16363 (2008), http://www.opticsinfobase.org/oe/abstract.cfm?URI=oe-16-21-16352.
10. E. Choi, J. Choi, and M. G. Kang, "Super-resolution approach to overcome physical limitations of imaging sensors: an overview," Int. J. Imaging Syst. Technol. **14**(2), 36–46 (2004).
11. C. Park, M. K. Park, M. G. Kang, S. C. Park, M. K. Park; and M. G. Kang, "Super-resolution image reconstruction: a technical overview," IEEE Signal Process. Mag. **20**(3), 21–36 (2003).
12. P. Vandewalle, L. Sbaiz, J. Vandewalle, and M. Vetterli, "Super-resolution from unregistered and totally aliased signals using subspace methods," IEEE Trans. Signal Process. **55**(7), 3687–3703 (2007).
13. D. Keren, S. Peleg, and R. Brada, "Image sequence enhancement using sub-pixel displacements," in *Proceedings of the 2006 IEEE Computer Society Conference on Computer Vision Pattern Recognition* (1988), pp. 742–746.
14. H. Stark, and P. Oskoui, "High-resolution image recovery from image-plane arrays, using convex projections," J. Opt. Soc. Am. A **6**(11), 1715–1726 (1989).
15. K. Nishiyama, M. Okita, S. Kawaguchi, K. Teranishi, and R. Takamatsu, "32" WXGA LCD TV using OCB Mode, low temperature p-Si TFT and blinking backlight technology," in *SID Tech. Dig.* **36**(1), 132–135 (2005).
16. S. Gauza, X. Zhu, W. Piecek, R. Dabrowski, and S. T. Wu, ""Fast Switching Liquid Crystals for Color-Sequential LCDs, " IEEE/OSA J, Display Technol. **3**(3), 250–252 (2007).

#116226 - $15.00 USD Received 25 Aug 2009; revised 15 Oct 2009; accepted 15 Oct 2009; published 1 Dec 2009

17. J. M. Liu, *Photonic Devices* (Cambridge University Press, 2005), Chap. 1.
18. J. J. Wang, J. Deng, X. Deng, F. Liu, P. Sciortino, L. Chen, A. Nikolov, and A. Graham, "Innovative high-performance nanowire-grid polarizers and integrated isolators," IEEE J. Sel. Top. Quantum Electron. **11**(1), 241–253 (2005).
19. Y. Ekinci, H. H. Solak, C. David, and H. Sigg, "Bilayer Al wire-grids as broadband and high-performance polarizers," Opt. Express **14**(6), 2323–2334 (2006), http://www.opticsinfobase.org/oe/abstract.cfm?URI=oe-14-6-2323.
20. R. Lu, X. Zhu, S. T. Wu, Q. Hong, and T. X. Wu, "Ultrawide-View Liquid Crystal Displays," IEEE/OSA J Display Technol. **1**(1), 3–14 (2005).
21. R. Raskar, A. Agrawal, and J. Tumblin, "Coded exposure photography: motion deblurring using fluttered shutter," ACM Trans. Graph. **25**(3), 795–804 (2006) (TOG).

1. Introduction

Image sensors have in recent years evolved from primarily image/video capture devices to "smart cameras" with real-time on-board processing functionality [1,2]. Along with continuously stronger embedded digital signal processing (DSP) capability and keen demands for high-quality imaging, new imaging systems named "computational cameras" have received great attention [3–9]. The concept of computational cameras is that an extra controllable optical or mechanical device is inserted into the traditional lens-detector configuration to generate sub-images with small variations, such as displacement [4–6], specific aberrations [7,8], and so on. Consequently, higher dynamic range [3], wider field of view [9], or even super-resolution (SR) images could be accomplished using a corresponding post-processing algorithm [4–8].

The most essential research topic in computational cameras is resolution enhancement, due to the constraint of sensor pixel density. The straightforward solution is to further reduce the pixel size of the image sensor; however, this is limited not only by the minimum feature size of the fabrication process, but also the degradation of image quality by shot noise [10]. However, based on the well developed SR algorithms [10–14], image resolution higher than sensor pixel density can be achieved via the reconstruction of several sub-pixel displaced images.

To achieve such sub-pixel image shifts, Nayar *et al.* attached actuators to mechanically control the image sensor with sub-pixel displacements [4]. However, the bulky size is not suitable to portable purposes, and the low response time of only 8 frames per second (fps) is not adequate for the 30 fps frame rate in common video applications. MEMS approaches in optical image manipulation have received considerable attention since the notable success of digital micro-mirror device (DMD) projectors, especially owing to their compact size and fast response time. Solgaard *et al.* utilized a 2-axis scanning micromirror to translate the image with sub-pixel shifts [6]; the compact device size and less than 10 milliseconds response time are very suitable to modern computational camera purposes. However, compared to the 3 millimeters or greater size of current image sensors, the working area of their micromirror is still too small, i.e. only 500 μm in diameter. Although they introduce a relay lens and modulate light beams on its back focal plane, this results in a more complicated and bigger imaging configuration, and also affects the image quality because high spatial frequencies away from the working area of the micromirror are lost.

In this work, we experimentally demonstrate a 2-dimensional sub-pixel image shifter, operating in transmission, which can translate images quickly and non-mechanically. Via the walk-off phenomenon from the birefringence of sapphire crystals, images with two polarization components are separated by a sub-pixel distance. A liquid-crystal (LC) waveplate combined with a linear polarizer acts as a non-mechanical switch to select between the sub-pixel displaced images. Moreover, in order to achieve two-dimensional image shifting, a second LC is sandwiched between two identical but orthogonally-aligned sapphire crystals; therefore, by controlling the voltage of the two LC layers, two-dimensional sub-pixel displaced images can be captured. LC cells have been widely used in display applications as controllable waveplates, possessing advantages such as fast response time [15,16], and low wavelength dependence. Based on these superior characteristics, manipulating images by LC control is very suitable for computational cameras because several different sub-images

#116226 - $15.00 USD Received 25 Aug 2009; revised 15 Oct 2009; accepted 15 Oct 2009; published 1 Dec 2009

should be taken in a very short time and most environmental light is chromatic. In addition, under the imaging configuration, this sub-pixel image shifter is simply placed between the lens and image sensor, as shown in Fig. 1(a). Compared to the off-axis reflective approach (e.g. with MEMS mirrors), this on-axis transmissive geometry leads to less induced aberration, compact size, and easy system assembly.

The content of this paper is organized into four parts. In Section 2, we illustrate the optical design of the device. The visible spectrum response and angular variation for the device are described in Section 3. The imaging evaluation, including displacement accuracy and SR image enhancement, is presented in Section 4. Finally, conclusions are drawn in Section 5.

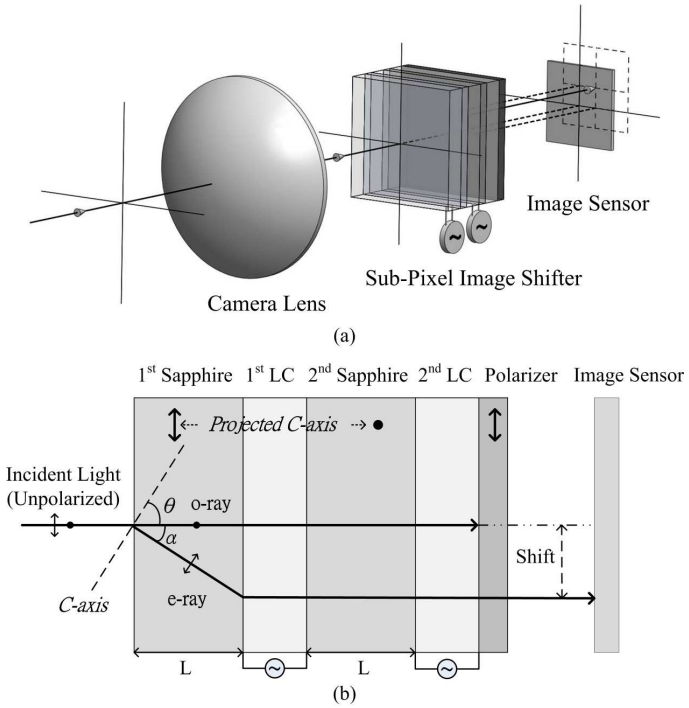

Fig. 1. (a) Schematic of the LC-controllable sub-pixel image shifter employed in a camera configuration. (b) Cross-section of the cascaded multi-layer structure.

2. Optical design

This sub-pixel image shifter is composed of five cascaded layers, including birefringent sapphire crystals, LCs, and a linear polarizer, as shown in Fig. 1(b). It can be further divided into two major parts: the first three layers from the left-hand side are used as a 2-dimensional sub-pixel image shifter, and the other two layers act as a polarization selective switch. The detailed working principle and component specifications are as follows.

As mentioned above, the walk-off phenomenon is employed to achieve the sub-pixel image shift. A major hypothesis for this device is that the incident lightwave is restricted to be unpolarized, which corresponds to the random polarization of most environmental light. After the unpolarized incident light impinges onto the birefringent crystal, the propagating direction of the ordinary ray (o-ray), whose polarization is perpendicular to the optical axis (C-axis) of the crystal as shown in Fig. 1(b), will follow Snell's law, and the extraordinary ray (e-ray), whose polarization is parallel to the C-axis, will be split from the original lightwave with a specific angle (α). By correct choice of thickness, the required sub-pixel displacement can be achieved. Double-side-polished R-plane sapphire crystals with a commercially available thickness of 1 mm were adopted here. Sapphire, a low dispersion material with a large Abbe number of 72.2, can avoid introducing chromatic variations into the device.

#116226 - $15.00 USD Received 25 Aug 2009; revised 15 Oct 2009; accepted 15 Oct 2009; published 1 Dec 2009

In this case, the splitting angle (α) between the o- and e-ray can be formulated as [17]:

$$\alpha = \tan^{-1}\left(\frac{n_o^2}{n_e^2}\tan\theta\right) - \theta \quad (1)$$

where n_o and n_e for sapphire crystal are 1.770 and 1.762, respectively, θ for R-plane crystalline orientation is 57.6°, and then a small splitting angle of 0.23° is derived. By simple triangularity, the displacement is approximately 4.1 μm with a sapphire thickness (L) of 1 mm. The experimental CCD image sensor has a pixel size of 7.4 μm, so that a displacement of 0.55 pixels is expected.

The LC cell used is of the type transmissive twisted nematic (TN), as mostly used for LCDs. As the lightwave is incident upon the LC, the polarization of the transmissive light will rotate by 90° in the voltage-off state. When a voltage of over 5V is applied, the liquid crystals are aligned with the applied field, and thus the polarization of the transmitting light ceases to be rotated. If the 1st LC is in the voltage-off state, the o- and e-ray coming from the 1st crystal remain as o- and e-rays with respect to the 2nd crystal, as a result of the polarization rotation by the LC combined with the mutually orthogonal alignment of the two crystals. Therefore, the image from the o-ray is fixed to the home-position, and the e-ray image is shifted with both tangential (from the 1st crystal) and sagittal (from the 2nd crystal) displacements. Because the above images have different polarizations, the 2nd LC plus a linear polarizer can be used as an image selector via simple LC voltage control.

Based on the same deduction, if the 1st LC is in the voltage-on state, the e-ray (in terms of the 1st crystal) is only shifted in the tangential direction, and the o-ray is translated in the sagittal direction by the 2nd crystal. As the polarization direction of the linear polarizer is parallel to the projected c-axis of the 1st crystal, the possible voltages for the two LC waveplates, and the corresponding expected shift values, are as denoted in Table 1.

Table 1. Expected displacement for the 4 operational states vs. LC voltage.

State Code	1st LC	2nd LC	Ideal Shift (in pixels)
A	Off	On	(0, 0)
B	Off	Off	(0.55, 0.55)
C	On	On	(0, 0.55)
D	On	Off	(0.55, 0)

3. Fabrication and characterization of sub-pixel image shifter

The cascaded device is simply assembled using an optical adhesive with refractive index around 1.5, which can avoid strong Fresnel reflections from the several interfaces and reduce ghost image problems. The orientation of the two sapphire crystals and the linear polarizer should be aligned carefully in order to achieve accurate polarization control. Ready-made LC waveplates with approximately 1 mm thickness were adopted here; each has the liquid crystal embedded between two glass plates on which transparent electrodes have been deposited. An adhesive plastic polarizer, as used in LCD panels, was chosen, with thickness approximately 0.5 mm. Therefore, the total thickness for this demonstrated device is less than 5 mm. This thickness could be reduced substantially by eliminating the glass plates of the LC cells, resulting in a highly miniature device which is compatible with most portable camera applications.

Since environmental lighting is chromatic, the sub-pixel image shifter should be wavelength-insensitive to ensure that the whole visible spectrum is well controlled. To examine the spectral response, a spectrometer (Model *Hitachi U-4100*) was employed with a linearly polarized light source, whose polarization is perpendicular to the linear polarizer in

#116226 - $15.00 USD Received 25 Aug 2009; revised 15 Oct 2009; accepted 15 Oct 2009; published 1 Dec 2009

the image shifter. Under such experimental arrangements, the A and D state are expected as a transparent result, and the other two states of B and C should be opaque. As shown in Fig. 2, the transparent spectra for A and D states reveal a high uniformity of 0.33 dB over the whole visible range, which indicates the polarization for all visible light can be well rotated by the LC waveplate. Therefore, the captured images on the image sensor have a low wavelength-dependent variation from this LC-based device. In addition, the insertion loss of this cascaded device was measured and found to be approximately 64% in all states. This can be attributed to the inherent 50% from the polarizer, and 14% excess loss from reflections and absorption.

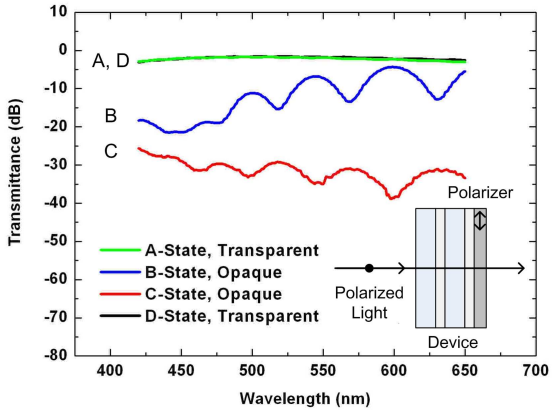

Fig. 2. Spectral response of the sub-pixel image shifter. The incident light is linearly polarized so as to examine the extinction ratio of the polarization switch.

The extinction ratio of the polarization switch is important because any light with the unwanted polarization that is captured by the image sensor will act as noise in the intended sub-pixel displaced image. The average difference between the transparent and opaque states indicates the extinction ratio of this device. As shown in Fig. 2, the difference between C and D state is up to 30.2 dB over the whole visible range. This result just fits the specification of the plastic polarizer. Normally, CCD or CMOS image sensors can provide dynamic range more than 40 dB; therefore, the admitted light with opposite polarization will somewhat affect our current device's performance, including the accuracy of image registration and the resolution improvement. In the future, utilizing other polarizer technologies with higher extinction ratios is a feasible solution; values more than 50 dB have been reported [18 19,]. However, the average difference between A and B state is only about 10.4 dB, significantly less than between C and D. The reason is that the polarization of the incident light is rotated twice by the two LC waveplates with both voltage-off operations, and that more serious wavelength-dependent variation is thus induced. Further design of the LC waveplates with wavelength compensation in multiple polarization rotations will be studied in the next configuration of the device. Fabry-Perot-like fringes can also be seen in Fig. 2, with a periodicity corresponding to a cavity of only a few microns thickness. The adhesive layer may account for this effect

Angle-dependent variation is also important because light from the image forming lens necessarily has a finite angular distribution. In order to examine this device's acceptable angular range, the same setup used for the spectral response was further employed to measure the transmittance for three primary colors as a function of incident angle from normal to 20°. The results for the first two states are shown in Fig. 3(a), and the other two states are in Fig. 3(b). As shown in Fig. 3(b), the average extinction ratio for all three colors steadily decreases, but still remains above 20.1 dB at 15°. This result is similar to the restricted viewing angles of LCDs because LC waveplates cannot precisely control the polarization rotation for those light beams with larger incident angles. In addition, the angular result for the B state is also worse than the C state, resulting from the same problem of multiple polarization rotations. In the following experiments for imaging evaluation, the camera lens operated at a focal length of 50

#116226 - $15.00 USD Received 25 Aug 2009; revised 15 Oct 2009; accepted 15 Oct 2009; published 1 Dec 2009

mm and an f-number of 3.5 was adopted. The maximum incident angle of the off-axis marginal rays in this configuration is approximately 10.7°, and the corresponding extinction ratio is still above 20 dB. To keep high extinction ratios and uniformity for wide-angle purposes, such as wide-angle cameras or smaller f-numbers, LCs with wide-viewing-angle technology [20] could be further introduced. Positioning the device at the aperture stop within the compound lens system could also be used to reduce the effects of angle dependence.

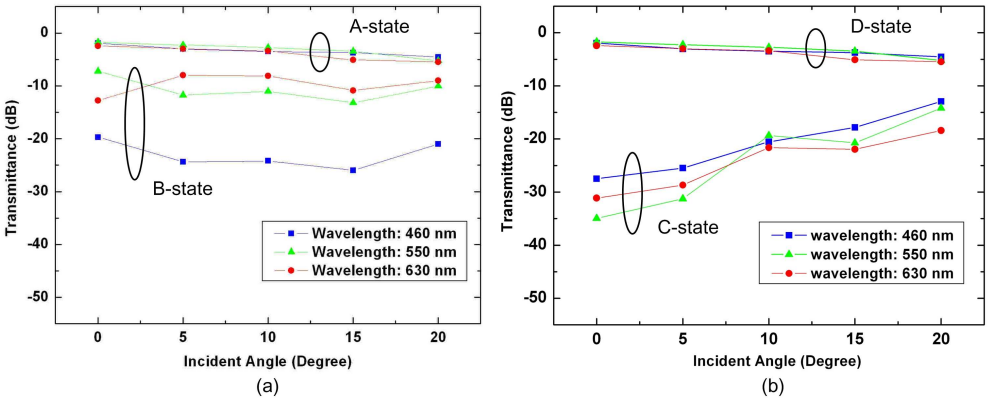

Fig. 3. Angle-dependent transmittance for three primary colors. The upper and lower three lines indicate the transparent and opaque state respectively. The results for the first two states are shown in (a), and the other two states are in (b).

4. Imaging evaluation and discussion of results

The experimental imaging setup is shown in Fig. 4. The sub-pixel image shifter with 5 mm thickness is inserted between the camera lens and the CCD image sensor (Model *IDS UI-2410SE*). The inset shows the top view of the image shifter, whose active area is larger than that of the image sensor. Two pairs of wires for the dual LC layers are connected to an AC voltage source with frequency of 1 KHz, which can avoid LC charge accumulation problems and maintain the stability of LC orientation during the image exposure time. The applied peak-to-peak voltage for voltage-on state is set to 10 V. An electronic circuit switches the different translation states, and sends trigger signals sequentially for each state to the image sensor, to take images synchronously in video form.

A star target with 0.6 ~14 pitch/mm wedge spacing was adopted in this experiment. Regarding the lighting source, we apply a daylight bulb as continuous, chromatic, and unpolarized illumination to imitate general environmental light. After aligning this imaging system, with optimized focusing, sub-images of the four translation states are taken sequentially via the control circuit. Figure 5(a) reveals 4 captured images with the original lower resolution of 385 × 385 pixels per frame. These images look very similar, indicating this image shifter provides low image distortion and variation for 4 different states.

#116226 - $15.00 USD Received 25 Aug 2009; revised 15 Oct 2009; accepted 15 Oct 2009; published 1 Dec 2009

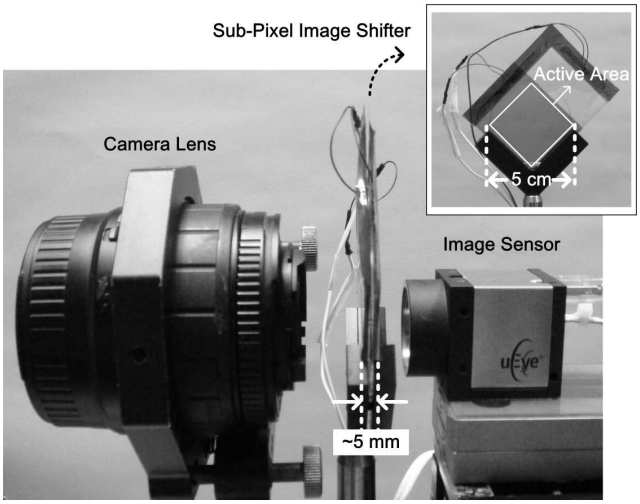

Fig. 4. Experimental imaging setup for the sub-pixel image shifter. The image shifter, with 5 mm thickness and wide working area, is placed between the camera lens and the image sensor.

To estimate the accuracy of sub-pixel displacement for the captured images, Keren's sub-pixel registration method [13] is employed. A series of sub-images for 4 states taken sequentially are analyzed, giving the image displacement in pixels, as shown in Fig. 5(b). Since sub-images are recorded in video form, a frame rate of 25 fps is chosen here, so that the time between frames is comfortably sufficient for the LC transition and the image exposure. The exposure time is set to much less than the value to reach saturation, in order to maintain contrast. The average displacements in horizontal and vertical directions are approximately 0.47 pixels, which has some deviation from the design shift of 0.55. Possible reasons for this might be the 5% thickness tolerance of the sapphire crystals, and assembly inaccuracy. The displacement variation is within 0.05 pixels, as indicated by the added circles in Fig. 5(b). Contributing factors to this small variation include computational inaccuracy and environmental vibration. Unlike other approaches [4–6] using mechanical movement of sensors or light beams, the image translations of our approach have been fixed by the properties of the birefringent sapphire crystals, providing very stable displacements based on the intrinsic optical characteristics of the material.

#116226 - $15.00 USD Received 25 Aug 2009; revised 15 Oct 2009; accepted 15 Oct 2009; published 1 Dec 2009

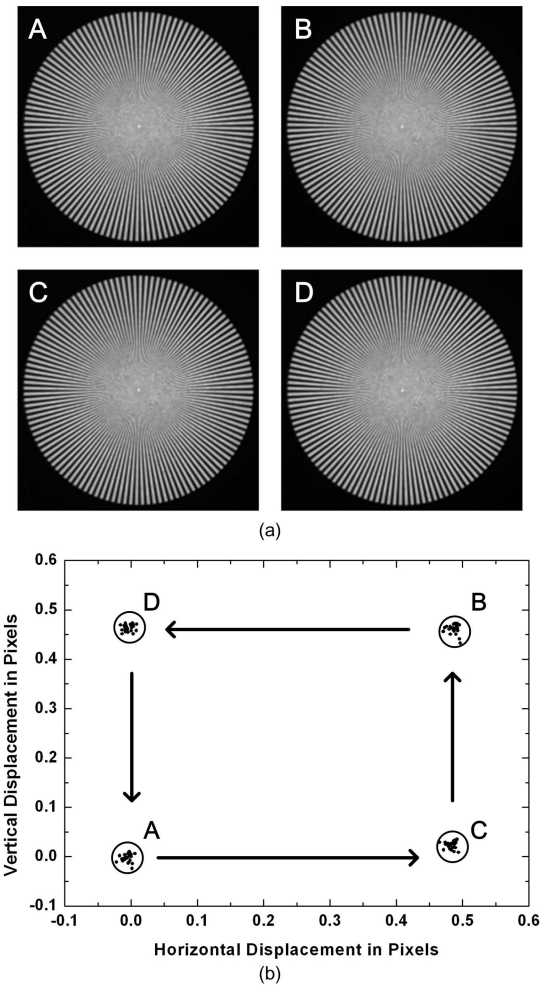

Fig. 5. (a) Captured images for A~D states by voltage control of two LC waveplates. Each frame has the original lower resolution of 385 × 385 pixels. (b) Illustration of the displacement accuracy of the image shifter. The displacement variation is indicated by the 0.05 pixel diameter of the added circles.

As shown in Fig. 6(a), the SR image with twofold up-sampling of 770 × 770 pixels is computed by the projection onto convex sets (POCS) algorithm [12,17]. This SR image maintains the image quality without sacrificing the sharpness after image magnification. In addition, the star wedge shapes also display good and similar performance in all directions. Figure 6(b) shows enlargement of the rectangular area marked with a white dashed line in Fig. 6(a), and a comparison of the same area calculated via the bi-cubic method. The bi-cubic image is up-sampled from one of the 4 originally captured images by an interpolation-based method. We can observe higher contrast in the SR image compared to the bi-cubic one. Especially for the region with smaller feature size, the pixels have higher and lower luminance values to depict the small variation.

Aliasing artefacts can be observed in Fig. 6(b), which result from the under-sampling of the image with respect to the diffraction limit, and the absence of anti-aliasing filters or other measures. To avoid such artefacts, while not preventing resolution enhancement by the sub-sampling, a practical implementation of this device should incorporate an anti-aliasing solution which is optimized to the specific characteristics of the sub-sampling and SR reconstruction.

#116226 - $15.00 USD Received 25 Aug 2009; revised 15 Oct 2009; accepted 15 Oct 2009; published 1 Dec 2009

The contrast transfer function (CTF), i.e. the variation of contrast ratio with spatial frequency for square wave modulation, is a convenient way to quantitatively measure the enhancement of spatial resolution by the SR technique. Therefore, the above star wedge images are further analyzed by measuring the contrast ratio along concentric circles from outer to inner radii sequentially. Figure 7 shows the CTF results for both SR and bi-cubic images. The ratio between the CTF values increases from low to high spatial frequency. At the highest spatial frequency of 2.61 lp/mm, the CTF ratio is enhanced by 1.36 times, from 19.5% to 26.5%. Because the magnification of the experimental imaging system is approximate 1/22, there are only 2.3 original pixels to resolve a single period at a spatial frequency of 2.61 lp/mm. After the SR reconstruction, this is increased to 4.6 effective smaller pixels. Thus, the better CTF performance of the SR image in the high spatial frequency region shows how displaced sub-images, through SR processing, can be equivalent to capturing images via a higher-resolution image sensor.

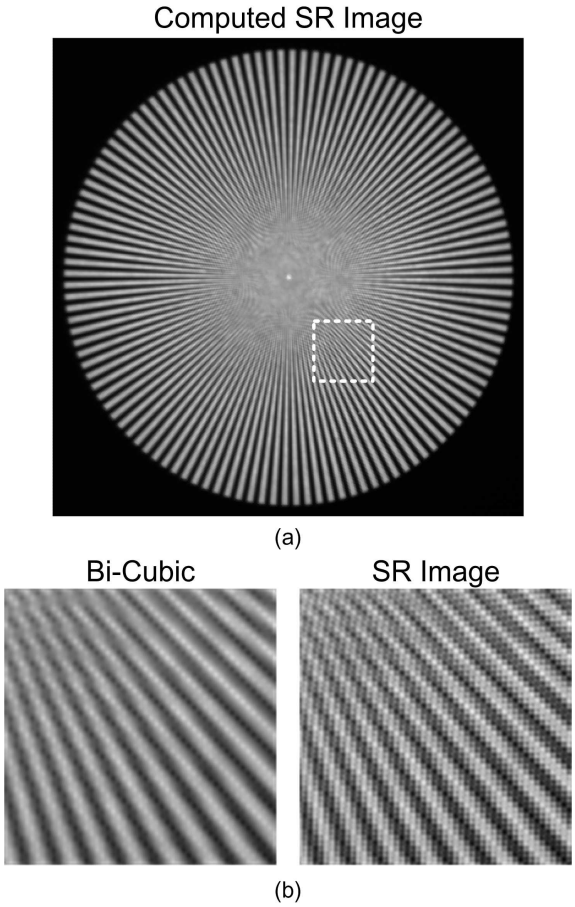

Fig. 6. (a) Computed SR image with twofold up-sampling of 770 × 770 pixels via POCS method. (b) Enlarged details for comparison between bi-cubic and SR images. The bi-cubic image is up-sampled from one of 4 originally captured images by an interpolation-based method.

#116226 - $15.00 USD Received 25 Aug 2009; revised 15 Oct 2009; accepted 15 Oct 2009; published 1 Dec 2009

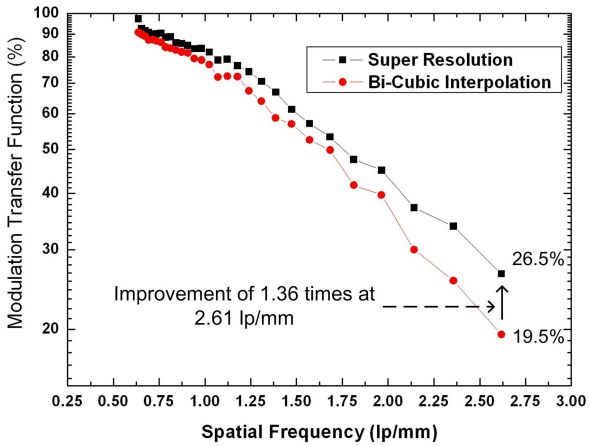

Fig. 7. CTF analysis for quantitative comparison between bi-cubic and SR images. The CTF improvement increases with spatial frequency.

Sub-pixel image shifters should have rapid response time. This not only reduces vibration effects, but also enables various applications such as motion deblurring [4,21] or high-resolution video with high frame rate [4], if suitable imaging processing algorithms are employed. Based on the short transition time with LC control, our device can rapidly switch the sub-images to different translation points.

Figure 8 shows the displacement accuracy of the image shifter operated at different frame rates. The 4 displacement states are recorded frame by frame as a video image sequence. The time used to capture a displaced sub-image includes image exposure duration (fixed to 5 ms for all conditions) and LC transit time (approximate 20 ms). The registration results in Fig. 8 reveal the displacement inaccuracy that results as the frame rate rises over 45 fps. This is because if the LC transit time is longer than the time to the next exposure, the oppositely polarized light, with incorrect displacement, is also captured. In this experiment, the adopted LC has a transition time of 20 ms, but ultra-rapid LCs of only 2~4 ms switching time have been widely applied in LCDs [15,16]; hence, frame rates of more than 60~80 fps should be feasible using current LC technologies.

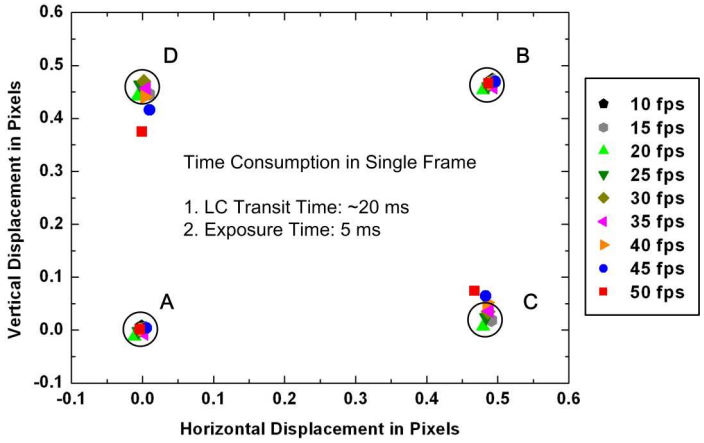

Fig. 8. Displacement accuracy for different frame rates. The sub-pixel image shifter can translate the sub-images with a frame rate up to 40 fps, limited by the 5 ms exposure time and approximate 20 ms LC transition time.

#116226 - $15.00 USD Received 25 Aug 2009; revised 15 Oct 2009; accepted 15 Oct 2009; published 1 Dec 2009

5. Conclusion

In this work, a sub-pixel image shifter using the walk-off phenomenon in birefringent sapphire crystals, and employing LC waveplates to switch between translation states, is experimentally demonstrated. Low wavelength dependence and acceptable angular range of convergent light beams are also shown. Displacement results for 2-dimensional image shifts with 4 different states show high accuracy, with variation less than 0.05 pixels. Regarding the imaging evaluation, the CTF ratio for the SR image in high spatial frequencies is enhanced by up to 1.36 times compared to an original captured image which is interpolated using the bi-cubic method. High-speed switching for each translation state is also demonstrated, with a frame rate of up to 40 fps, which could be further improved by use of ultra-rapid LCs. These characteristics suggest that this non-mechanically controlled device with compact size could have potential as a sub-pixel image shifter in computational camera configurations.

The operational principle of this device assumes that the light entering the imaging system is unpolarized, so that the image splitting in the birefringent crystals produces equal intensities in each polarization. In practice, some reflected light, e.g. from oblique flat surfaces or from certain artificial materials, can have a significant degree of linear polarization. This will produce differences in contrast among the shifted images, which will reduce the performance of the super-resolution computations. Some reduction in such effects might be obtained by aligning the image shifts along the diagonal directions, since many cases of linearly polarized reflections will have polarization axes in the vertical-horizontal directions, and thus will produce equal intensities if split by a crystal with diagonal principal axes. Computational correction approaches should also be explored.

From the working principle of the SR algorithm, more sub-pixel displaced images would result in SR images with more accurate pixel values or higher up-sampling factors. This sub-pixel image shifter has the potential to generate more sub-images with different displacements, by inserting additional specific birefringent crystals and LC waveplates into the cascaded structure. Of course, the increasing LC layers would also introduce more wavelength dependence, although this might be overcome by the LC-layer design to compensate the optical path differences for the whole visible spectrum. Additional insertion loss would also result from cascading additional stages. Alternatively, other electro-optic modulation techniques, such as Pockels cells, could achieve more displacement values within a pixel range, although high control voltages would likely be required.

Acknowledgements:

The authors greatly appreciate the assistance of Mr. Chia-Yu Lee, Department of Optics and Photonics, National Central University, Taiwan, and Mr. Sam Harrasi, Department of Electrical & Electronic Engineering, Imperial College London, UK, in developing the device assembly and control circuit, respectively. We would also like to thank Prof. Guang-Zhong Yang for suggesting work on sub-pixel shifters for computational cameras. Finally, one of us (Hsiao-Chin Lan) also thanks the Graduate Student Study Abroad Program (GSSAP) of the National Science Council, Taiwan, for funding his research at Imperial College London.

#116226 - $15.00 USD Received 25 Aug 2009; revised 15 Oct 2009; accepted 15 Oct 2009; published 1 Dec 2009